International Journal of Mechanical and Production Engineering Research and Development (IJMPERD)
ISSN(P): 2249-6890; ISSN(E): 2249-8001
Vol. 8, Issue 6, Dec 2018, 667-680

THE THERMAL ANALYSIS OF FIVE-PHASE PMSG FOR SMALL-SCALE WIND POWER APPLICATION

RAJA RAM KUMAR, S. K. SINGH, R. K. SRIVASTAVA & R. K. SAKET

Indian Institute of Technology, Banaras Hindu University, Varanasi, Uttar Pradesh, India

ABSTRACT

Unlike the conventional three-phase PMSG, the five-phase PMSG has a higher power density. This paper presents a lumped parameter thermal model of Five-Phase Permanent Magnet Synchronous Generator (FP-PMSG) for small-scale Wind Energy Conversion (WEC) system. The purpose of this thermal analysis is to use it for the optimal selection of various materials required for development of FP-PMSG. Two methods, namely Finite Element Method (FEM) and Lumped Parameter Model (LPM) applied here for the thermal analysis. The FEM results are more accurate, but time consuming where as LPM provides results in less time. Eight different nodes corresponding to critical parts of the machine are considered in LPM to estimate the temperature of stator yoke, winding, magnet, rotor yoke and shaft under natural cooling. The predicted LPM results are found in good agreement with the simulated FEM, based on which specific materials are identified for various sections of FP-PMSG.

KEYWORDS: Wind Power, Five-Phase, Permanent Magnet synchronous Generator, Lumped Parameter Thermal Model & Finite Element Method

Received: Oct 12, 2018; **Accepted:** Nov 02, 2018; **Published:** Dec 06, 2018; **Paper Id.:** IJMPERDDEC201869

Original Article

1. INTRODUCTION

In the current scenario, wind energy is popular, clean and echo-friendly renewable energy source [1], [2]. To harness the wind power a high power density, reliable and efficient conversion system is required. PMSG is a quite suitable wind power conversion system because it has advantages like high power density, improved reliability and high efficiency, and it doesn't require slip-ring or gear box like conventional systems [3] -[5]. The power density, fault tolerance capability and reliability of the conversion system can be further enhanced using multi-phase (more than three phases) system. The multi-phase system eliminate the higher order harmonics from generated voltage and therefore required DC link capacitor size is reduced [6], [7]. The multi - phase system also offers a higher degree of freedom under fault operation than three phase system [8], [9]. These advantages of multi-phase system motivated the authors to explore the thermal design aspect of FP-PMSG. The electromagnetic and thermal analysis decides the output power, life span and reliability of PMSG [10]. The stator winding insulation and permanent magnets are the most critical temperature sensitive parts of the generator. The frequent overheating not only reduces the life span of winding insulation, but also partially demagnetizes the permanent magnets of the machine [11]. A persistent overheating may lead to complete demagnetization of permanent magnets that would eventually lead to complete failure of generator [12]. Therefore, thermal analysis is a very important step to ensure optimum thermal design. There are two approaches for thermal modelling namely numerical technique and lumped parameter technique [13]. Among numerical techniques, finite element method (FEM) is quite popular. It is very accurate with higher resolution but

inconvenient and time consuming for design optimization [14]. The lumped parameter technique is fast, simple and reasonably accurate [15]. Most researchers utilize this technique for computation of either steady state temperature or both steady state and transient state temperature [10] -[15].

The prime focus of this paper is to present the thermal model for five phase permanent magnet generator. The lumped parameter technique is considered for fast, simple and precise prediction of temperature distribution. The conductive thermal resistance, convective thermal resistance and the thermal capacitance enable the model to predict the transient and steady state temperature. Since the thermal behaviour of the winding is very difficult to predict so the process of calculation of thermal resistance between winding and stator core is also discussed. The predicted results from lumped parameter model are verified with simulated FEM results. Furthermore, these results are utilized for the selection of appropriate materials for various sections of FP-PMSG including permanent magnet, winding insulation and core laminations.

This Paper is organised in the following manner. Section-2 describes the schematic model, winding detail and the design parameters for FP-PMSG. Section-3 elaborates the thermal network model, different losses in the model and equivalent thermal parameter of the model. Section-4 describes the FEM model and their results are used to validate the predicted result from lumped parameter model as discussed in section-5. Finally, section-6 draws the concluding remarks.

2. SIZE AND DESCRIPTION OF FIVE PHASE PMSG

Figure 1 shows the schematic model of 60 slots, 8pole, five-phase PMSG. It consists of stator and surface mounted permanent magnet rotor. Stator core is made up with thin laminations of high grade silicon steel alloy and these laminations are insulated from each other with high thermal resistant paper or varnish. The stator core houses the five phase double layer fractional slot short-pitched winding, which reduces the higher order space harmonics. The 8 permanent magnets are mounted on the rotor surface. The 8 poles of the rotor are conformed by 8 flux loops which are shown in Figure 2. The rating of the designed generator is listed in Table 1 and corresponding dimensions are listed in Table 2.

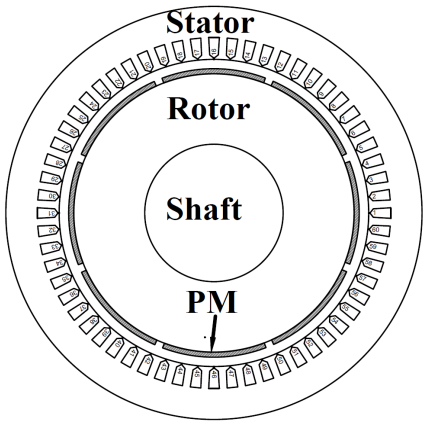

Figure 1: Schematic of Proposed Generator

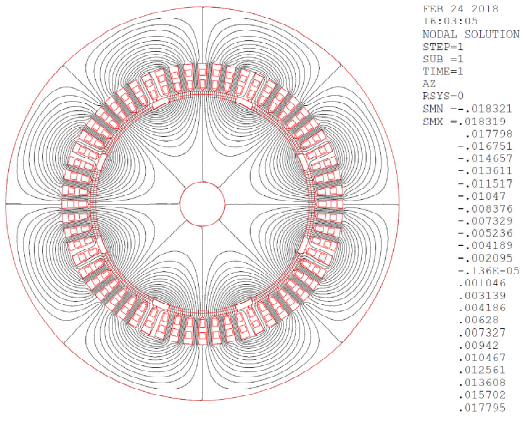

Figure 2: Conforming Eight Poles of Proposed Generator

Table 1: Rating of Generator

Parameter	Value
Power (kva)	3.878
Voltage (Volt)	193.92
Current (Amp)	4
Speed(rpm)	400

Table 2: Dimension Details of the Generator

Parameter	Value
Radius of Shaft	20 mm
Outer radius of rotor	95 mm
Height of magnet	2.5mm
Airgap length	2.5 mm
Inner radius of stator	100 mm
Outer radius of stator	175 mm
Area of slot	125 mm^2

3. LUMPED PARAMETER THERMAL NETWORK MODEL

The lumped parameter thermal network is shown for proposed FP-PMSG in the Figure 3. There are 8 nodes in the network and the thermal resistances are connected between these nodes. In addition, the thermal capacitance, heat flow effect and heat generating sources are included in the model. Depending on the heat transfer mode the thermal resistances are divided into three categories, namely conduction, convection and radiation, but radiation is not considered in the model because it has very less effect for small rating machines. The thermal resistances and thermal capacitances in the network from right to left are namely convective thermal resistance of shaft to the environment (Rsh_nc), conductive thermal resistance (Rsh), conductive thermal resistance of the upper and lower part of rotor yoke (Rryu and Rryl), conductive thermal resistance of the upper and lower part of PM (Rpmu and Rpml), conductive thermal resistance of air between the two magnets (Rpm_air), conductive thermal resistance of air (Rair), convective thermal resistance between rotor to air (Rar_nc), conductive thermal resistance between the winding and core(Rsw), conductive thermal resistance of lower and upper part of tooth (Rsti and Rstu), conductive thermal resistance of lower and upper part of stator yoke (Rsyl and Rsyu) and convective thermal resistance of stator yoke and environment (Rsy_nc) and the thermal capacitance of rotor yoke(Cry), thermal capacitance of permanent magnet (Cpm), thermal capacitance of copper winding (Ccu), thermal capacitance of stator tooth (Cst) and thermal capacitance of stator yoke (Csy). The heat sources are mainly due to the losses of stator winding (Pcu), Permanent magnet (Ppm), stator yoke (Psy), stator tooth (Pst) and rotor yoke (Pry). The ambient temperature (Ta) is taken as 30ºC.

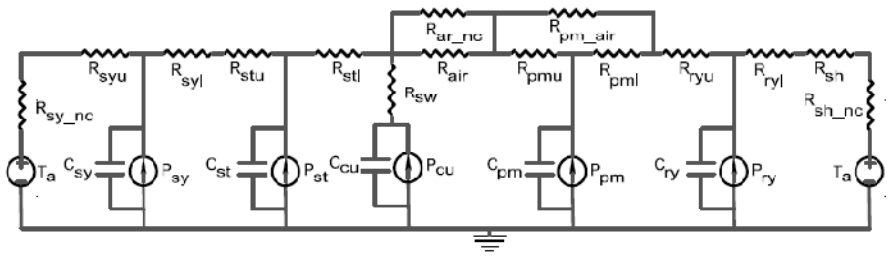

Figure 3: Lumped Parameter Model

The following assumptions are taken during thermal modelling:

- Materials are anisotropic in nature.
- The heat generation and thermal capacity are uniformly distributed in the model
- The heat flow in axial and radial direction is independent to each-other.
- The circumferential heat flow in the model is absent.

3.1 Thermal Conductive Resistance and Thermal Capacitance

For the steady state thermal analysis the thermal equilibrium equation can be written as follows.

$$[G][T]=[P] \tag{1}$$

Where [G] is the thermal conductance matrix of the generator, [T] is the temperature rise of different nodes in the model and [P] is the loss matrix of the generator.

The thermal conduction resistance between the nodes i and j:

$$R_{i,j}=\frac{l}{kA} \tag{2}$$

Where l is the path length of conductive media, A is the area of cross-section and k is the thermal conductivity of material.

Thermal capacitance(C) can be expressed as

$$C=\rho V c_p \tag{3}$$

Where c_p is the specific heat, ρ is the material density and V is the volume of cylindrical region.

3.2 Equivalent Thermal Resistivity between Stator Slot Winding and Core

The thermal resistivity between the stator core and winding are different in different side of slot, this is due to insulating layer and dimensional variation. The stator slots consists of impregnated copper conductor, wedge, paper insulation of slot liner, and insulating material between the two layers of winding, so the thermal conductivity between the stator core to winding is not easy to define. Reference [10] suggests the possible approach to compute the thermal resistance as well as the equivalent thermal conductivity of winding impregnation and slot insulation.

The equivalent thermal conductivity(k_{eq}) can be expressed as

$$k_{eq}=\frac{\sum_{i=1}^{n} t_i}{\sum_{i=1}^{n} \frac{t_i}{k_i}} \tag{4}$$

Where t_i is the thickness of different insulating layer and k_i is their respective thermal conductivity for the insulating material.

The equivalent thermal resistance between the winding and stator core are different in different parts because of dimensional variation.

The conductive thermal resistance between winding and stator core is calculated as

$$R_{wc} = \frac{t_{wc}}{k_{eq} A_{wc}} \tag{5}$$

Where t_{wc} is the insulation thickness in the heat flow direction, A_{wc} is the cross-section area of contact between the insulation and core.

3.3 Thermal Conductive Resistance

Convection is due to the variation of air density at the convective surface. Two types of convection are possible from the surface, namely natural convection and forced convection. For the natural cooled machine, the outer stator to environment interface surface and the axial shaft to environment interface surface have natural convection, whereas the stator teeth to the rotor interface surface can be natural or forced convection depending on the laminar and turbulent flow of heat.

The Convective thermal resistance can be expressed as

$$\mathrm{R} = \frac{1}{h_c A} \tag{6}$$

Where h_c is the convective heat transfer coefficient and A is the area of convective surface.

$$\mathrm{h}_c = \frac{\mathrm{N}_u k_{air}}{\delta} \tag{7}$$

N_{uh} is the nusselt number and K_{air} is the thermal conductivity of air and δ is the characteristic length. The empirical formula for nusselt number varies and depends on the natural and forced convection of heat from the surface [16].

For natural convection the nusselt number (N_{uc}) is

$$\mathrm{N}_{uc} = a\left(G_r P_r\right)^b \tag{8}$$

For force convection the nusselt number (Nuf) is

$$\mathrm{N}_{uf} = a R_e^b P_r^c \tag{9}$$

Where a, b and c are the constant, G_r is the grash of number, P_r is the prandtl number and R_e is the reynold number.

The empirical equations of nusselt number used for the outer stator to environment interface surface N_{uh} and the axial shaft to environment interface surface N_{uv} are expressed as

$$N_{uh} = \left(0.6 + 0.387 R_a^{0.166} \left(1 + 0.721 P_r^{-0.5625}\right)^{-0.296}\right)^2 \quad (10)$$

$$N_{uv} = \left(0.825 + 0.387 R_a^{0.166} \left(1 + 0.671 P_r^{-0.5625}\right)^{-0.296}\right)^2 \quad (11)$$

$$R_a = G_r P_r = \frac{g\beta(T_s - T_\infty)\delta^3}{\upsilon^2} P_r \quad (12)$$

$$P_r = \frac{c_p \mu}{k_{air}} \quad (13)$$

Where R_a is the Rauleigh number, ν is the kinematic viscosity of air, g is the acceleration of gravity (m/sec^2), β is the coefficient of cubic expansion, T_s is the surface temperature(^{o}C), T_∞ is the temperature(^{o}C) of air, δ is the characteristic length, c_p is the specific heat capacity at constant pressure(kJ/kg.^{o}C).

The nusselt number used for the stator teeth to rotating rotor interface surface is decided by the reynold number and it depends on the speed of rotor. If the reynold number is less than the critical value (10^5) then the convective heat flow is laminar otherwise it is turbulent.

The reynold number (Re) is calculated as

$$R_e = \frac{\pi \rho_{air} N_r (\delta)^2}{60\mu} \quad (14)$$

Where N_r is the rotor speed (rpm), ρ_{air} is the air density(Kg/m^3), μ is the dynamic viscosity (Kg/sec.m)of air. The calculated value of reynold number in this paper is 4.67x10^4 which is less than the critical value of reynold number. The heat flow is therefore laminar and comes under natural convection.

The empirical formula of nusselt number used for the stator teeth to rotor interface surface N_{uLa}.

$$N_{uLa} = \frac{0.886 R_e^{1/2} P_r^{1/2}}{\left(1 + \left(\frac{P_r}{0.0207}\right)^{2/3}\right)^{1/4}} \quad (15)$$

Using equation (10), (11) and (15) the convective heat transfer coefficient for the outer stator to environment interface surface, axial shaft to environment interface surface and the stator teeth to rotating rotor interface surface are 23.4014, 4.9263 and 958.3188(w/m^2.k), respectively.

3.4 Loss Calculation in Different Parts of the Model

Core loss in the stator yoke, stator tooth and rotor yoke can be calculated as

3.4.1 Stator Core Loss

Iron loss in stator yoke is expressed as

$$P_{sy} = k_e f^2 B_{sy}^2 + k_h f B_{sy}^2 + k_a f^{1.5} B_{sy}^{1.5} \tag{16}$$

Iron loss in stator tooth is expressed as

$$P_{st} = k_e f^2 B_{st}^2 + k_h f B_{st}^2 + k_a f^{1.5} B_{st}^{1.5} \tag{17}$$

Where k_e is the coefficient of eddy current constant, k_h is the coefficient of hysteresis constant, k_a is the coefficient of excess loss constant, B_{sy} is the peak flux density in the iron core, B_{st} is the peak flux density in the stator tooth and f is the frequency(Hz).

3.4.2 Copper Loss of Stator Winding

The copper loss is the prime contributor to loss in PM machine, it is due the resistivity of copper wire in the per phase winding.

The total copper loss in the winding can be expressed as

$$P_{cu} = \sum_{m=1}^{5} I^2 R_{ph} \tag{18}$$

where I is the phase current R_{ph} is the phase resistance and m is the number of phases.

3.4.3 Rotor Loss

The rotor loss is divided into two parts namely core loss and permanent magnet loss. The rotor core loss is due to the eddy current loss, hysteresis loss and excess loss in the rotor whereas the permanent magnet loss is due to the eddy current developed in it. The rotor core loss can be calculated by the following formula

$$P_{ry} = k_e f^2 B_{ry}^2 + k_h f B_{ry}^2 + k_a f^{1.5} B_{ry}^{1.5} \tag{19}$$

Where B_{ry} is the peak flux density in the rotor core.

The procedure and the expression developed for eddy current loss for permanent magnet is mentioned in [17] and [18]. The conductivity for the NdFeB is 7.7×10^5 s/m.

Permanent magnet loss is calculated as

$$P_{pm} = w_e^2 \left(\sum_{k=1}^{\infty} B_g^2 \right) \frac{N_a N_c V_{pm} m_\delta^3}{16 \rho_{pm} \left(C_{eff} + m_\delta^2 \right)} \frac{\frac{W_{pm}}{N_c}}{\frac{L_{pm} N_c}{W_{pm} N_a}} \left(\frac{1}{2} + \frac{2}{3} \frac{\left(2C_{eff} + m_\delta^2 \right) \left(\frac{L_{pm} N_c}{W_{pm} N_a} - m_\delta \right)}{m_\delta \left(C_{eff} + m_\delta^2 \right)} + \frac{C_{eff}^2 \left(\frac{L_{pm} N_c}{W_{pm} N_a} - m_\delta \right)^2}{m_\delta^2 \left(C_{eff} + m_\delta^2 \right)} - \frac{2C_{eff}^2 \left(\frac{L_{pm} N_c}{W_{pm} N_a} - m_\delta \right)^3}{m_\delta \left(C_{eff} + m_\delta^2 \right)^3} + \frac{2C_{eff}^2 \left(\frac{L_{pm} N_c}{W_{pm} N_a} - m_\delta \right)^4}{\left(C_{eff} + m_\delta^2 \right)^4} \ln \left(1 + \frac{C_{eff} + m_\delta^2}{m_\delta \left(\frac{L_{pm} N_c}{W_{pm} N_a} - m_\delta \right)} \right) \right) \tag{20}$$

where w_e is the electrical angular speed (rad/sec), B_g is the flux density, N_a is the number of axial segment, N_c is the number of arcillier segment, V_{pm} is the volume of magnet, ρ_{pm} is the resistivity of magnet, m_o is the slope of line passing through the path of eddy current edge, $C_{eff}(\geq 1)$is the factor of incremental path length of eddy current, L_{pm} is the length of permanent magnet and W_{pm} is the width of permanent magnet.

4. FINITE ELEMENT MODEL ANALYSIS

The finite element model analysis has been done using ANSYS software. This method requires a fast processor with the high storage device and took around two hours for simulation but it is highly accurate. In this paper, there are two solver used for the thermal analysis, namely harmonic analysis and transient analysis. These analyses are performed by setting element type (quad 4, node 13), degree of freedom, material properties and meshing the model into 227720 elements. The harmonic analysis uses an AZ degree of freedom for the elements when calculating the losses and heat generation rate in different parts of the model. The heat generation rate which is store in.rmg file from this analysis is further used for the thermal analysis. The elemental degree of freedom Temp is used for the thermal analysis. The analysis type (transient), time at the end of load step (86400 sec), load heat generation from Mag Analysis, boundary condition (Convection), is taken in solution step. The results of Temperature distribution, radial temperature distribution and heat flux plot are shown in postprocessor step.

Figure 4 shows the temperature distribution in the model and it is found that the winding temperature is highest whereas the shaft temperature is least. Since the machine is naturally cooled so the heat is released to the environment via outer stator surface and the shaft. Although, the convective area of the shaft is less than the outer stator, but the shaft temperature 113.869^{o} C is less than the outer stator yoke temperature 119.231^{o} C this is because of conduction of heat from winding to outer stator yoke is higher.

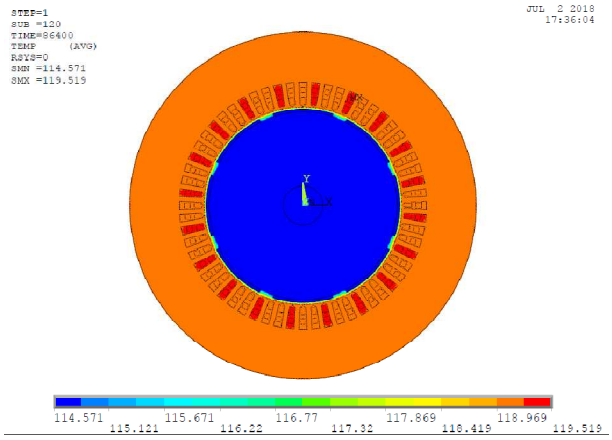

Figure 4: Temperature Distribution in the Model

Figure 5 shows the temperature rise in different parts of the model. The FEM simulation runs for 24 hours and the steady state temperature is attained by the model in around 16 hours.

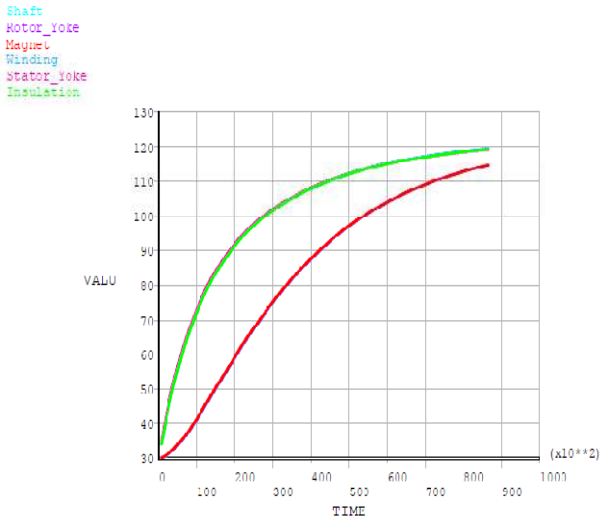

Figure 5: Temperature Developed in the Model

The radial temperature distribution is shown in figure 6. The temperatures of the shaft and rotor yokes are found at the same level because of heat transfer in conduction mode. A sharp increment is found at winding and it decreases at the stator yoke surface due to convection process to the environment.

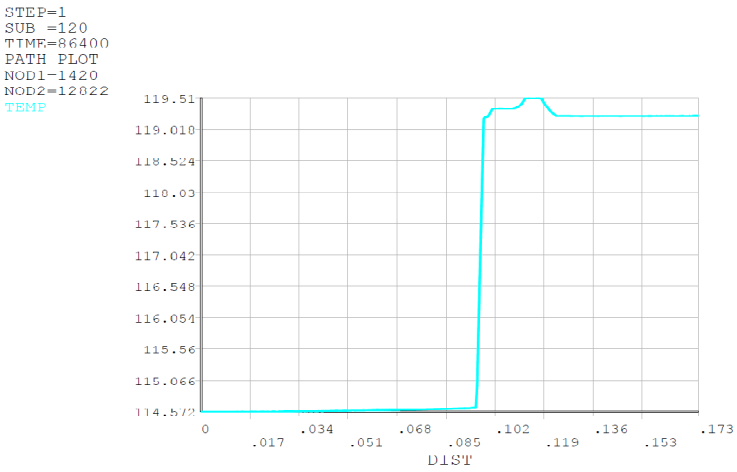

Figure 6: Radial Temperature Distribution

5. RESULT AND VALIDATION

The predicted temperature using the lumped parameter method for shaft is shown in figure 7. It is observed that the settling time to attain steady state temperature is comparatively lower for LPM than FEM. The estimated steady state temperature of the shaft is 113.869ºC. The shaft temperature effects the bearing lubrication and could lead towards reduced viscosity or increased friction. This effect requires regular monitoring and maintenance else deteriorated bearings could eventually result in an eccentricity fault of the machine.

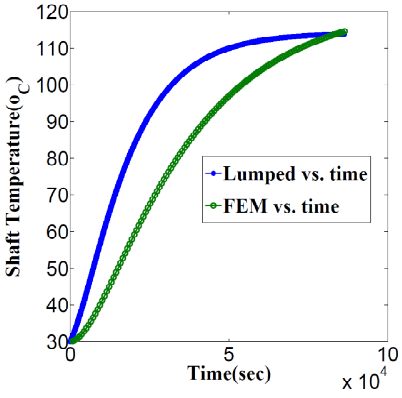

Figure 7: Shaft Temperature

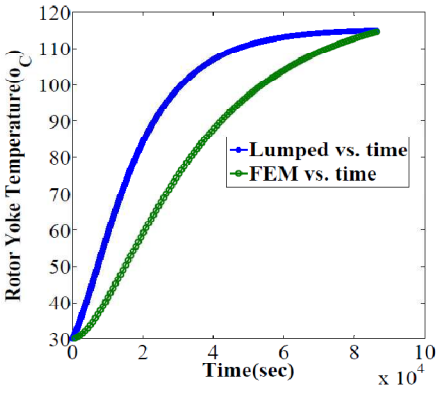

Figure 8: Rotor Yoke Temperature

Figure 8 shows that the steady state temperature of the rotor yoke is 114.997ºC. Lamination of the rotor yoke is required to reduce the eddy current loss due to armature reaction. For this a thin layer of insulation is placed between the cores. Table 3 lists the insulation materials for lamination and corresponding maximum operating temperature. The Class B insulating material is therefore appropriate for rotor yoke lamination.

Table 3: Yoke Insulation Materials

Material (Silicon Resins Laminated)	Temperature (^{O}C)
Class A (Impregnated Varnished)	105 (max)
Class B	130-155
ClassF	155-180
ClassH	180-200

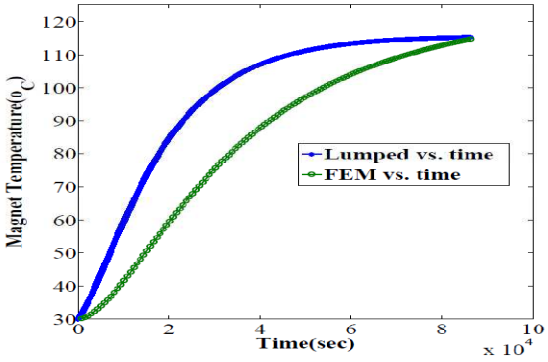

Figure 9: Magnet Temperature

The permanent magnet temperature is shown in Figure 9. For the NdFeB magnets the steady state temperature is 115.151ºC.

Table 4: Different Grade of NdFeB Permanent Magnet

PM material	Maximum Operating Temperature(^{O}C)
NdFeB N	80
NdFeB M	100
NdFeB H	120
NdFeB SH	150

Table 4: Contd.,	
NdFeB UH	180
NdFeB EH	200

Different grade of NdFeB permanent magnets is shown in Table 4. For the proposed FP-PMSG the NdFeB H grade magnet seems appropriate.

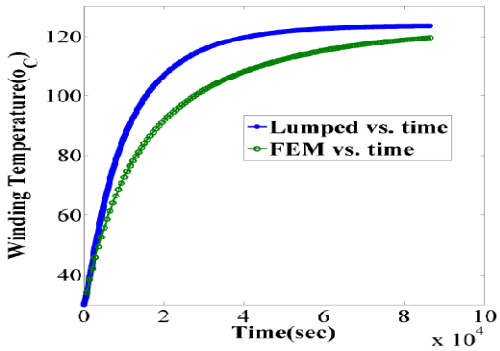

Figure 10: Winding Temperature

The maximum temperature of the FP-PMSG appears at the winding. For the proposed machine the steady state winding temperature is 123.528ºC as shown in Figure 10. Appropriate winding insulation is mandatory to ensure safe operation of the machine.

Table 5: Winding Insulation

Material Used for Winding	Maximum Attainable Temperature(^{O}C)
Class A	105
Class E	120
Class B	130
Class F	155
ClassH	180

The list of winding insulating materials is shown in Table 5. The class B winding insulating material is the optimum material for this purpose.

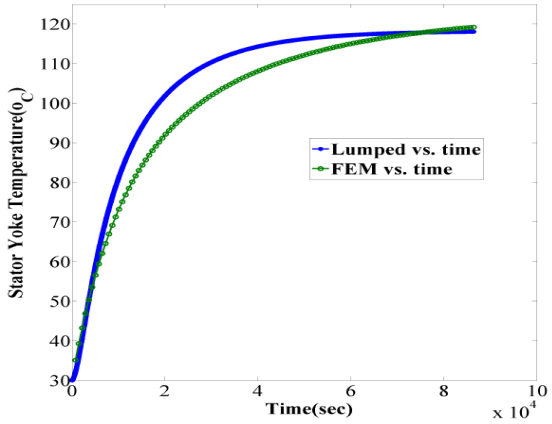

Figure 11: Stator Yoke Temperature

The temperature builds up process in the stator yoke is shown in Figure 11. From this figure the steady state temperature of the stator yoke is 118.063ºC. Using Table 3, the Class B insulating material is the appropriate choice for

stator yoke laminations.

In a comprehensive manner the estimated temperature of the various sections of the proposed FP-PMSG using LPM and FEM is presented in Table 6. The percentage error between the predicted temperature result using LPM and FEM results are very close. This confirms the capability of the lumped parameter model in analysing quick and reasonably accurate results for the proposed FP-PMSG.

Table 6: Steady State Temperature of Different Part of PMSG

Parameter	Lumped	FEM	%Error
Shaft	113.869	114.572	-0.617
Rotor Yoke	114.997	114.597	0.347
Magnet	115.151	114.632	0.45
Winding	123.528	119.510	3.253
Stator Yoke	118.063	119.231	-0.989

6. CONCLUSIONS

This paper presented a lumped parameter model, which is a simple and fast technique for predicting the temperature distribution inside the proposed FP-PMSG. The thermal behaviour of the windings in the slot is not easy to compute so the technique for computing the equivalent conductive thermal resistances between the winding and the core is discussed. The permanent magnet is the most sensitive part of the machine so losses in it are discussed in detail. Based on the predicted temperature various materials are identified for the development and safe operation of the machine. This includes class B insulating material for stator and rotor yoke laminations, class B insulating material for windings and NdFeB H grade material as permanent magnets. Maintenance issues due to shaft temperature on bearing lubrication viscosity are also highlighted. The error between the predicted and FEM are found within the 4 % limit which ensure the accuracy of predicted results using the lumped parameter model for the proposed FP-PMSG.

REFERENCES

1. *Nektarios E. Karakasis and Christos A. Mademlis "High efficiency control strategy in a wind energy conversion system with doubly fed induction generator" Renewable Energy, Vol. 125, Page-974 – 984, September 2018.*
2. *Sener Agalar and Yusuf Alper Kaplan "Power quality improvement using STS and DVR in wind energy system" Renewable Energy, VOL. 118, Page-1031 – 1040, April 2018.*
3. *M. Kimura, D. Kori, A. Komura, H. Mikami, K. Ide, T. Fujigaki, M. Iizuka and M. Fukaya "A Study of Permanent Magnet Rotor for Large Scale Wind Turbine Generator System" IEEE International Conference on Electrical Machines, pp. 1161-1171, 2012.*
4. *A. Tani, Y. Gritli, M. Mengoni, L. Zarri, G. Sala, A. Bellini and G. Serra "Detection of Magnet Demagnetization and High-Resistance Connections in Five-Phase Surface-Mounted Permanent Magnet Generators" IEEE 10th International Symposium on Diagnostics for Electrical Machines, Power Electronics and Drives (SDEMPED), pp. 487-493, 2015.*
5. *Ahmed M. Hemeida, Wael A. Farag, and Osama A. Mahgoub "Modeling and Control of Direct Driven PMSG for Ultra Large Wind Turbines", World Academy of Science, Engineering and Technology, International Journal of Energy and Power Engineering, Volume- 5, issue-11, pp. 1269–1275, 2011.*
6. *Govardhan, D., & Praveen, B. Design And Analysis of Two Throat Wind Tunnel.*

7. *SalaheddineRhaili ; Ahmed Abbou ; Saloua Marhraoui and Nezha El Hichami "Vector Control of Five-phase Permanent Magnet Synchronous Generator based Variable-Speed Wind Turbine" IEEE International Conference on Wireless Technologies, Embedded and Intelligent Systems (WITS), pp. 1-6, 2017.*
8. *Raja Ram Kumar, S.K. Singh, R. K. Srivastava "Design Analysis of Radial Flux Dual Stator Five Phase Permanent Magnet Synchronous Generator" IEEE International Conference on Power Electronics, Drives and Energy Systems (PEDES), PP. 1-6,2014.*
9. *NgacKy Nguyen, Fabien Meinguet, Eric Semail, and Xavier Kestelyn: "Fault-Tolerant Operation of an Open-End Winding Five-Phase PMSM Drive With Short- Circuit Inverter Fault", IEEE Transactions on Industrial Electronics, Volume-63, issue-1, pp. 595–605, 2016.*
10. *FatihaMekri, Seifeddine Ben Elghali, and Mohamed El Hachemi Benbouzid "Fault-Tolerant Control Performance Comparison of Three- and Five-Phase PMSG for Marine Current Turbine Applications" IEEE Transactions On Sustainable Energy, Vol. 4, No. 2, pp.425-433, 2013.*
11. *Wenming Tong, Shengnan Wu and Renyuan Tang "Totally Enclosed Self-Circulation Axial Ventilation System Design and Thermal Analysis of a 1.65-MW Direct-Drive PMSM" IEEE Transactions On Industrial Electronics, Vol. 65, No. 12, Page-9388 – 9398, December 2018.*
12. *Raja Ram Kumar, Santosh K Singh and R K Srivastava "Thermal Modelling of Dual-Stator Five-Phase Permanent Magnet Synchronous Generator" IEEE Transportation Electrification Conference (ITEC-India), page-1-6, 2017.*
13. *XiuhuaCai, Ming Cheng, Sa Zhu, and Jiawen Zhang "Thermal Modeling of Flux-Switching Permanent-Magnet Machines Considering Anisotropic Conductivity and Thermal Contact Resistance" IEEE Transactions On Industrial Electronics, Vol. 63, No. 6, pp. 3355-3365, 2016.*
14. *Bin Zhang, Ronghai Qu, Jin Wang, Wei Xu, Xinggang Fan, and Yu Chen "Thermal Model of Totally Enclosed Water-Cooled Permanent-Magnet Synchronous Machines for Electric Vehicle Application" IEEE Transactions On Industry Applications, Vol. 51, No. 4, pp.3020-3029, 2015.*
15. *Claudio Sciascera, Paolo Giangrande, Luca Papini, Chris Gerada and Michael Galea "Analytical Thermal Model for Fast Stator Winding Temperature Prediction" IEEE Transactions On Industrial Electronics, Vol. 64, No. 8, pp.6116-6126, 2017.*
16. *Aldo Boglietti, Andrea Cavagnino,, David Staton, Martin Shanel, Markus Mueller, and Carlos Mejuto "Evolution and Modern Approaches for Thermal Analysis of Electrical Machines" IEEE Transactions On Industrial Electronics, Vol. 56, No. 3, pp.871-882, 2009.*
17. *David A. Staton and Andrea Cavagnino "Convection Heat Transfer and Flow Calculations Suitable for Electric Machines Thermal Models" IEEE Transactions On Industrial Electronics, Vol. 55, No. 10, pp.3509-3516, 2008.*
18. *Peng Zhang, Gennadi Y. Sizov, Jiangbiao He, Dan M. Ionel and Nabeel A. O. Demerdash "Calculation of Magnet Losses in Concentrated-Winding Permanent-Magnet Synchronous Machines Using a Computationally Efficient Finite-Element Method" IEEE Transactions On Industry Applications, Vol. 49, No. 6, pp. 2524-2532, 2013.*
19. *Wan-Ying Huang, Adel Bettayeb, Robert Kaczmarek, and Jean-Claude Vannier "Optimization of Magnet Segmentation for Reduction of Eddy-Current Losses in Permanent Magnet Synchronous Machine" IEEE Transactions On Energy Conversion, Vol. 25, No. 2, pp.381-387, 2010.*